Influence of doping density on electronic transport in degenerate Si:P δ-doped layers

K. E. J. Goh,* L. Oberbeck,† and M. Y. Simmons
Australian Research Council Centre of Excellence for Quantum Computer Technology, School of Physics, University of New South Wales, Sydney, New South Wales 2052, Australia

A. R. Hamilton and M. J. Butcher
School of Physics, University of New South Wales, Sydney, New South Wales 2052, Australia
(Received 14 October 2005; published 3 January 2006)

We present a detailed study addressing the effect of doping density on electronic transport in Si:P δ-doped layers grown by phosphine dosing and low temperature molecular beam epitaxy. We demonstrate that the surface P coverage can be determined directly from scanning tunneling microscope analysis of PH_3 dosed Si(100) surfaces, with good quantitative agreement to that measured by Auger electron spectroscopy. For samples with doping densities between $\sim 1\times 10^{13}$ cm^{-2} to $\sim 5\times 10^{14}$ cm^{-2}, we found that mobility decreases with higher doping. In contrast, both the mean free path and phase coherence length increase with doping density up to a maximum at a room-temperature saturation dose of phosphine ($\sim 2\times 10^{14}$ cm^{-2}). We discuss the implications of our results for the fabrication of nanoscale Si:P devices by scanning probe lithography and phosphine dosing.

DOI: 10.1103/PhysRevB.73.035401 PACS number(s): 81.16.−c, 75.47.−m, 68.37.Ef, 85.35.Ds

I. INTRODUCTION

Recent demonstrations[1,2] of highly conducting Si:P nanowires ($\sim$25 nm wide with four-terminal resistances of $\sim$50 kΩ at 4 K) fabricated by scanning probe lithography highlight the future potential for this fabrication technology towards atomic scale devices. In view of this, it is important to understand the range of both the electronic mean free path l and phase coherence length l_φ achievable in order to determine the possibilities of ballistic and phase coherent transport in Si:P nano-scale to atomic-scale devices.

The study of Si:P δ-doped layers with different doping densities provides an important precursor to understanding how both l and l_φ scale for 2D transport in Si:P devices fabricated by scanning probe lithography. Previous studies[3,4] of Si:P δ-doped layers with P doping levels of $\sim 10^{14}$ cm^{-2} have shown that l is of the order of a few nm with a corresponding transport relaxation time τ in the femtosecond range. In contrast, l_φ at the same doping density exceeds 100 nm (at temperatures <1 K) with a corresponding phase relaxation time τ_φ of the order of picoseconds.

In this paper, we present a systematic study of the electronic transport in Si:P δ-doped samples fabricated using phosphine (PH_3) and low-temperature molecular beam epitaxy (MBE) over the doping range of $\sim 1\times 10^{13}$ cm^{-2} to $\sim 5\times 10^{14}$ cm^{-2}. The P densities were determined from a combination of Auger electron spectroscopy and scanning tunneling microscope (STM) analysis of PH_3 dosed Si(100) surfaces. We compare our results with a recent Si:P δ-doping study[3] which unexpectedly shows a conflicting mobility trend from those reported for Si:Sb and Si:B δ-doped layers[5] for a similar range of densities studied. In addition, we present the doping density dependence of both l and l_φ and discuss their implications for the fabrication of nanoscale Si:P devices using the STM.

II. EXPERIMENTAL

Experiments were performed in a custom-built UHV combined MBE-STM system. Both the MBE and STM chambers have been adapted for samples of size 1×1 cm^2 and have base pressures $<1\times 10^{-10}$ mbar. For high quality Si growth, the MBE chamber is equipped with an electron-beam Si evaporator. Auger electron spectroscopy (AES) was used in conjunction with STM analysis to determine the P coverage after PH_3 dosing.

All samples were cleaved from the same phosphorus-doped Si(100) wafer with resistivity ~ 5 Ω cm. Each sample underwent a standard sulphuric peroxide and RCA-II clean before being loaded into the MBE system. A clean and atomically flat starting surface was prepared by outgassing the sample at 600 °C for 30 min and 950 °C for 15 min followed by the growth of a $\sim$100 nm of undoped Si buffer at 650 °C using a rate of 1 Å s^{-1}.[6] Phosphorus doping was achieved by exposing the Si(100) surface to PH_3 via a precision leak valve at a pressure of $\sim 1\times 10^{-9}$ mbar for different times followed by an anneal to 500 °C to incorporate the P atoms and desorb the H atoms.[7] Finally, the P atoms were encapsulated by $\sim$50 nm of Si at a rate of 1 Å s^{-1} using low temperature Si MBE at 250 °C to suppress P segregation.[4] For magnetotransport measurements, the samples were fabricated into Hall bars and measurements were carried out at 4.2 K using standard low frequency ac lock-in techniques.

III. DETERMINATION OF P COVERAGE

Figure 1(a) is a filled state STM image of a typical starting Si(100)2×1 surface. This image shows the Si atoms reconstructing to form dimer rows with $\sim$7% of two common defect species: dimer vacancies and C defects.[8] We identify these initial features to distinguish them from surface species arising from PH_3 dosing.

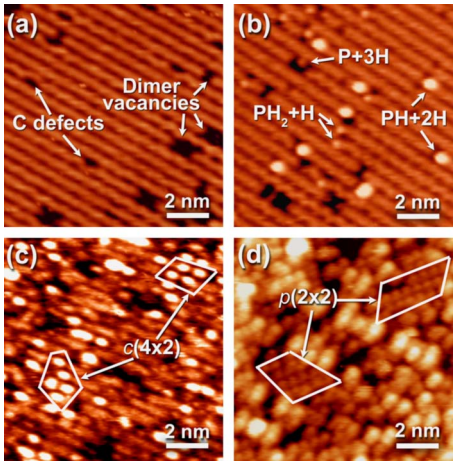

FIG. 1. (Color online) Filled state STM images of (a) a starting Si(100) surface at −1.9 V and room temperature PH_3 dosed Si(100) surfaces at −2.2 V for doses of (b) 0.018, (c) 0.27, and (d) 1.4 L.

Figures 1(b)–1(d) are filled state STM images from room temperature (RT) dosed samples with PH_3 doses of 0.018, 0.27, and 1.4 L, respectively. Here, a PH_3 dosing pressure of $\sim 1 \times 10^{-9}$ mbar was used and different doses were achieved by varying the dose time. We used a combination of AES and STM analysis to calibrate the surface P coverage against PH_3 dose [measured in langmuir (L)$=1.33 \times 10^{-6}$ mbar s]. The Auger P ratio was calculated from the ratio of the P signal to the (P+Si) signal.[9] In order to obtain a quantitative measure of the P coverage from the Auger measurements, we calibrated the Auger P ratio against a direct determination of the absolute P coverage from the identification of PH_x related species in the STM images of a PH_3 saturation dosed Si(100). Figure 1(b) highlights the surface species present after a low PH_3 dose of 0.018 L. It is now well established that PH_3 adsorbs dissociatively on the Si(100) from $PH_3 \rightarrow$asymmetric $PH_2+H \rightarrow$centered $PH+2H \rightarrow$U-shaped $P+3H$.[10] We can identify these PH_x features on the surface which are labeled in Fig. 1(b) and thereby determine the P coverage. At moderate dose levels [e.g., 0.27 L in Fig. 1(c)], there is a higher competition for available surface sites which limits the extent to which PH_3 can dissociate. As such we find a majority of PH+2H features which cluster into a $c(4 \times 2)$ ordering shown in Fig. 1(c). At a saturation dose of 1.4 L, the lack of available sites further limits dissociation as evidenced by the significant number of PH_2+H features which order in local regions exhibiting a $p(2 \times 2)$ reconstruction [Fig. 1(d)]. By counting the P-related features in STM images across several areas of each sample and averaging, we find the corresponding P coverages to be (b) 0.017, (c) 0.13, and (d) 0.33 monolayers (ML).[11] At a saturation dose of PH_3, we obtained an Auger P ratio of 0.17 corresponding to a P coverage of 0.33 ML determined from STM analysis. We used the ratio of these two values to scale the Auger data in order to obtain a calibration curve for P coverage against PH_3 dose.

Figure 2 shows good quantitative agreement between the AES measurements and statistical analysis of STM images for RT PH_3 doses up to a saturation coverage. From this calibration curve, we can now determine the P coverage from PH_3 dosage without interrupting the sample growth for STM imaging. The determination of P coverage from this calibration curve introduces an error of ~10% due to the uncertainties in the Auger and STM analysis.

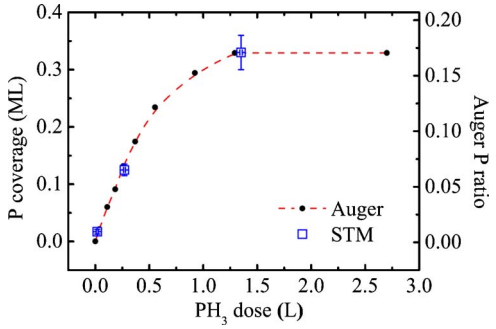

FIG. 2. (Color online) Surface P coverage calibrated by AES and STM analysis. The dashed line is a guide to the eye.

In this study, we are primarily interested in RT PH_3 dosing since this is compatible with the fabrication of nanodevices using STM lithography on H:Si(100).[12,13] Six samples N1–N6 were fabricated using RT PH_3 dosing. However, from Fig. 2 the maximum P coverage achievable using RT PH_3 dosing is only ~0.33 ML. In an attempt to increase the doping density further, we fabricated an extra sample N7 by dosing with ~1.5 L of PH_3 at 550 °C. Here, a P coverage of 0.77 ML is expected based on a previous statistical analysis of P-P, Si-P dimers observed by STM.[14] Prior to encapsulation, samples N1–N6 were annealed to 500 °C to incorporate the P atoms in substitutional lattice sites and desorb any H on the surface as this is known to enhance carrier activation and transport mobility.[7,15] For a sample with a low PH_3 dose of 0.06 L (or ~0.03 ML P coverage based on our calibration curve in Fig. 2), our AES measurements did not detect any difference in P coverage before and after the 500 °C anneal. This agrees with previous studies of PH_3 dosed Si(100) showing that P coverages less than ~0.1 ML remain intact for anneals up to ~600 °C.[9,16] However, for saturation dosed samples (~0.33 ML), we observed a 6% reduction in the AES signal for P after the 500 °C anneal. We attribute this reduction to the recombinative desorption of PH_3 which has resulted in a corresponding decrease of P coverage from 0.33 to 0.31 ML for our saturation dosed samples.[17]

IV. ELECTRONIC TRANSPORT

The electrical characteristics for samples N1–N7 are summarized in Table I. Sample N1 with the lowest doping of 1.2×10^{13} cm^{-2} gave non-Ohmic behavior with a sheet resistance of $\rho_{xx} \sim 1$ MΩ $\square^{-1}$. For doping $>2 \times 10^{13}$ cm^{-2}, our samples show Ohmic conductivity. Our data therefore suggests that a transition from strong to weak localization for Si:P δ-doped layers occurs in the vicinity of 1×10^{13} cm^{-2}, similar to that observed for Si:Sb δ-doped layers.[18]

For the Ohmic samples N2–N7, the 2D carrier densities n_{Hall} obtained from 4.2 K Hall-effect measurements are summarized in Table I and compared to the P coverage in Fig. 3.

TABLE I. Characteristics of Si:P δ-doped samples at 4.2 K.

Sample	N1	N2	N3	N4	N5	N6	N7
N_D (10^{14} cm^{-2})[a]	0.12	0.27	0.48	0.91	1.9	2.1	5.2[b]
n_{Hall} (10^{14} cm^{-2})		0.23	0.41	0.85	1.9	2.0	1.2
ρ_{xx} (kΩ $\square^{-1}$)	$\sim 10^3$	5.0	3.2	2.0	0.94	0.87	1.5
μ (cm^2 V^{-1} s^{-1})		56	48	37	35	36	34
l (nm)		4.4	5.1	5.7	8.0	8.4	6.2
τ (fs)		13	12	7.7	6.8	6.9	6.8
τ_φ (ps)		0.56	0.72	0.99	1.2	1.2	0.98
l_φ (nm)		26	36	52	80	82	59

[a]P coverage.
[b]From Ref. 14.

Samples N2–N6 exhibit almost complete electrical activation (where a P atom occupies a substitutional lattice site and gives up its free electron for conduction) while sample N7 with a P coverage of $\sim 5\times 10^{14}$ cm^{-2} shows only about $\sim$20% activation. The significant reduction of dopant activation in sample N7 is attributed to the formation of inactive P-related precipitates or dopant-vacancy complexes which are known to cause the reduction/saturation of electrical activity in heavily doped semiconductors where the number of dopants exceed the solubility limit in Si.[19]

The analysis of electronic transport in samples with P densities $>1.4\times 10^{13}$ cm^{-2} is complicated by occupation of at least six subbands.[20] For such degenerately δ-doped samples, however, strong intersubband scattering is expected[21,22] and it is therefore possible to ignore valley degeneracies and adopt a single subband approximation.[18,21,23] For the purpose of comparing transport trends, it is important to note that this approximation does not alter the functional form of the magnetotransport.[24] In all cases, we assume an electron effective mass $m^*=0.315\ m_e$.[25]

In Fig. 4 we present the sheet resistance ρ_{xx}, mobility μ and mean free path l as a function of n_{Hall} for our samples in zero magnetic field. Figure 4(a) shows that ρ_{xx} decreases as n_{Hall} is increased. Here the increase in the number of carriers dominates the electronic transport despite a corresponding increase in the number of ionized dopant scattering centers.

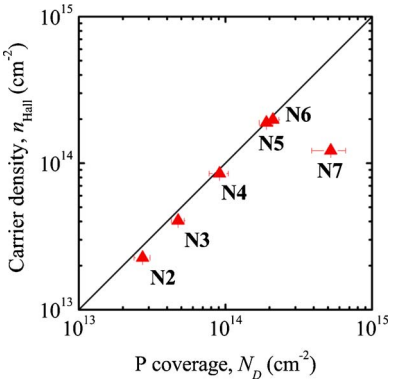

FIG. 3. (Color online) Hall carrier densities for samples N2–N7 vs P coverage. The solid line corresponds to complete electrical activation.

Similar trends for ρ_{xx} have been reported for Si:B (Ref. 21) and Si:Sb (Ref. 18) δ-doped layers [included in Fig. 4(a) for comparison] fabricated using low-temperature MBE.

The mobility for each δ-doped layer was calculated using $\mu=(\rho_{xx}n_{\mathrm{Hall}}e)^{-1}$. Figure 4(b) shows that μ decreases with n_{Hall}. The decrease in μ is ascribed to the increased impurity scattering as a consequence of the higher in-plane dopant density. While this trend is similar to those previously reported[5] for Si:Sb and Si:B δ-doped samples, it contrasts with a recent Si:P δ-doping study by Zudov *et al.*,[3] where the highest μ of $\sim$38 cm^2 V^{-1} s^{-1} was found at an intermediate n_{Hall} of 0.88×10^{14} cm^{-2}.

In Fig. 4(c), the mean free path l is observed to increase with n_{Hall}. At first, this may seem counterintuitive as l may be expected to decrease as the number of in-plane scatters increases. However, $l\propto\mu\sqrt{n_{\mathrm{Hall}}}$, so any decrease in μ is offset by the relatively larger effect of increasing n_{Hall}. This implies that a higher doping density is favorable for achieving a longer l in degenerately δ-doped layers. However, when we

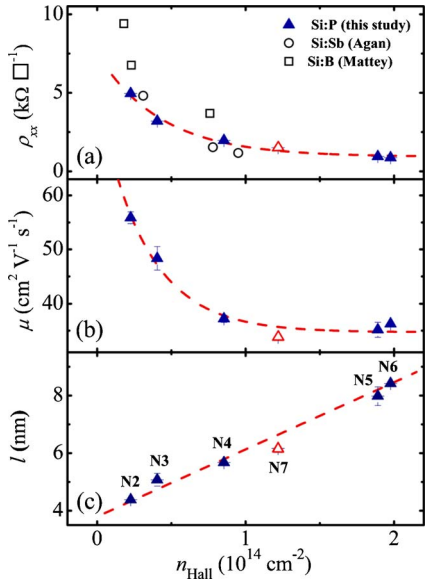

FIG. 4. (Color online) (a) Sheet resistance ρ_{xx} from this study compared with those from Si:Sb (Ref. 18) and Si:B (Ref. 21) δ-doped systems, (b) mobility μ, and (c) electronic mean free path l against carrier density n_{Hall}. Dashed lines are guides to the eye.

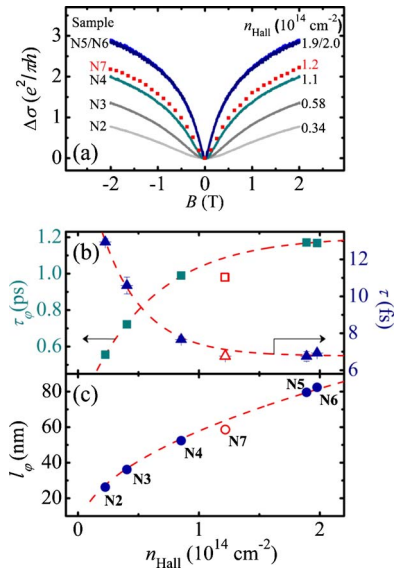

FIG. 5. (Color online) (a) Magnetoconductivities $\Delta\sigma(B)$ for Si:P δ layers, (b) transport (τ) and phase (τ_φ) relaxation times as a function of sheet density n_{Hall}, and (c) phase-coherent length (l_φ) as a function of n_{Hall}. Dashed lines are guides to the eye.

try to increase the PH_3 dose to ~0.8 ML, as in sample N7, donor activation is severely curtailed and n_{Hall} drops to 1.2×10^{14} cm^{-2}. Nevertheless, we see that the values of ρ_{xx}, μ, and l for sample N7 all appear to fit the respective general trends. While this suggests that the inactive dopants do not contribute significantly to electron scattering, it also highlights that no further transport enhancement is derived from such a high level of doping. For doping STM patterned areas, saturation PH_3 dose at RT represents the highest achievable n_{Hall} and the longest l as demonstrated by sample N6 ($n_{\mathrm{Hall}}\sim2\times10^{14}$ cm^{-2}).

We now turn our attention to magnetotransport properties in order to extract the phase relaxation time τ_ϕ and the phase coherence length l_ϕ which are important for fabricating devices which exploit quantum interference. Figure 5(a) shows plots of the magnetoconductivities

$$\Delta\sigma(B) = \frac{1}{\rho_{xx}(B)} - \frac{1}{\rho_{xx}(0)} \tag{1}$$

for the samples N2–N7 in a perpendicular magnetic field B. The inverted peak at $B=0$ is characteristic of weak localization arising from the interference of electron waves in time-reversed trajectories. The application of a perpendicular B breaks the time-reversal symmetry resulting in the release of electrons from localized trajectories[26] and this is reflected by the increase in $\Delta\sigma$ with B for each sample as shown in Fig. 5(a). Over a range of 2 T, the overall change in $\Delta\sigma$ is observed to increase with n_{Hall}. This behavior, as we shall show in the following analysis, is a reflection of the enhancement of phase coherent transport with higher carrier density n_{Hall}.

To obtain τ_ϕ and l_φ, we used the formulation by Hikami[27] for a disordered 2D system

$$\delta\sigma_{\mathrm{WL}}(B) = -\frac{\alpha e^2}{\pi h}\left[\Psi\left(\frac{1}{2}+\frac{B_0}{B}\right) - \Psi\left(\frac{1}{2}+\frac{B_\varphi}{B}\right)\right], \tag{2}$$

where α is a phenomenological prefactor, Ψ is the digamma function, and B_0 and B_φ are, respectively, the characteristic magnetic fields associated with transport and phase relaxation rates. By fitting $\Delta\sigma$ to $\delta\sigma_{\mathrm{WL}}(B)-\delta\sigma_{\mathrm{WL}}(0)$, we determine

$$\tau = \frac{\hbar}{4DeB_0} \quad \text{and} \quad \tau_\varphi = \frac{\hbar}{4DeB_\varphi} \tag{3}$$

from which we calculate the phase coherence length using $l_\varphi=\sqrt{D\tau_\varphi}$, where $D=\frac{1}{2}v_F\tau$ is the diffusion constant and v_F is the Fermi velocity. The values of τ, τ_φ, and l_φ extracted from fitting our data to Eq. (2) are summarized in Table I and plotted as a function of n_{Hall} in Figs. 5(b) and 5(c). In all cases, we obtained α within the range 1.2 to 1.4 indicating that the observed magnetoconductivity is primarily related to weak localization.[28,29]

Figure 5(b) shows that as n_{Hall} increases, τ decreases as expected [mirroring the behavior of μ in Fig. 4(b)]. However, τ_φ is observed to increase with n_{Hall}. At low temperatures, the dominant dephasing mechanism in a 2D system is electron scattering from the fluctuating potential of all moving electrons (Nyquist noise).[30] This leads to a universal material independent formula for τ_φ:

$$\frac{1}{\tau_\varphi} = -\frac{kT}{2\hbar}\frac{e^2}{\pi\hbar}\rho_{xx}\ln\frac{e^2}{\pi\hbar}\rho_{xx}. \tag{4}$$

As we saw earlier in Fig. 4(a), ρ_{xx} shows a general decrease with increasing n_{Hall}. Equation (4) implies that for Nyquist dephasing, as ρ_{xx} decreases, τ_φ should increase. This is in agreement with the general increase of τ_φ with n_{Hall} as shown in Fig. 5(b). Quantitatively however, we find that the theoretical values of τ_φ based on Eq. (4) are larger than our experimental values in Fig. 5(b) by a factor of ~15. Note that similar discrepancies between the theory and experiment have also been previously observed.[30,31] We have found that this factor may be reduced by using a larger electron effective mass and/or a valley degeneracy greater than 1 in our calculations. The observed discrepancy between the values of the measured and theoretical τ_φ may therefore arise from our effective mass and/or single subband approximations.

In Fig. 5(c), l_φ is observed to increase with n_{Hall}. As $l_\varphi \propto \sqrt{n_{\mathrm{Hall}}\tau\tau_\varphi}$, we expect l_φ to depend on n_{Hall}, τ and τ_φ. A careful study of Fig. 5(b), however, reveals that as n_{Hall} is increased, the decrease in τ is compensated by the increase in τ_φ. Hence, l_φ depends primarily on n_{Hall} which therefore accounts for the increase in l_φ with n_{Hall}.

For sample N7, despite its low electrical activation, the values for τ_φ and l_φ lie within ~10% of the main trend lines. Although this suggests that the inactive dopants do not contribute significantly to dephasing, it is clear that the higher P density in sample N7 does not further enhance phase coherent transport because of the inability to achieve a higher carrier density.

To summarize, the longest l_φ is attained at a doping density of $\sim 2\times 10^{14}$ cm^{-2} corresponding to a saturation dose of PH_3 at RT. For STM fabrication of Si:P devices that exploit phase coherent transport, a saturation dose of PH_3 is therefore advantageous. In fact, at temperatures <1 K, l_φ is observed to increase further to ~ 200 nm for our PH_3 saturation dosed sample N6.

V. CONCLUSION

In conclusion, we have studied the effect of doping density on electronic transport in Si:P δ-doped layers fabricated by phosphine dosing and low temperature molecular beam epitaxy. While room temperature PH_3 dosing is favored for its compatibility with STM lithography on H:Si(100), we have also investigated PH_3 dosing at 550 °C in order to achieve a higher P coverage. This enables us to analyze the transport trends over a wider doping range ($\sim 1\times 10^{13}$ cm^{-2} to $\sim 5\times 10^{14}$ cm^{-2}). For RT PH_3 dosed samples, we demonstrate that the P coverage determined by STM analysis based on P-related surface species[10] is in good quantitative agreement with AES measurements.

We observe that only samples with doping densities $>2\times 10^{13}$ cm^{-2} exhibit Ohmic conductivity and the highest 2D electron density n_{Hall} of $\sim 2\times 10^{14}$ cm^{-2} is achieved by a saturation dose of PH_3 at RT. At a very high P coverage of ~ 0.8 ML (or $\sim 5\times 10^{14}$ cm^{-2}), electrical activation is significantly reduced to $\sim 20\%$ due to the formation of deactivating precipitates/defects. In contrast to the recent study of Si:P δ-doped samples by Zudov *et al.*,[3] we find that the mobility decreases monotonically with n_{Hall}. However, our mobility trend is in agreement with existing reports for Si:Sb and Si:B δ-doped samples.[5] Most importantly, we show that both the mean free path l and phase coherence length l_φ increase with carrier density up to a maximum of ~ 10 and ~ 100 nm, respectively, using a RT saturation dose of PH_3. For STM device fabrication, a RT saturation dose of PH_3 is thus expected to maximize the upper limits of the length scales for both ballistic and phase coherent transport. Our results imply that STM fabricated Si:P devices that exhibit ballistic transport are limited to a length scale of several nanometers while those exploiting phase coherent transport can be at least an order of magnitude longer.

ACKNOWLEDGMENTS

K.E.J.G. acknowledges financial support from A*STAR (Singapore). This work was supported by the Australian Research Council, the Australian Government, the Semiconductor Research Corporation, the U.S. Advanced Research and Development Activity, the National Security Agency, and the Army Research Office under Contract No. DAAD19-01-1-0653.

*Electronic mail: jgoh@phys.unsw.edu.au
†Now with Infineon Technologies AG.

[1] T.-C. Shen, J. S. Kline, T. Schenkel, S. J. Robinson, J. Y. Ji, C. Yang, R. R. Du, and J. R. Tucker, J. Vac. Sci. Technol. B **22**, 3182 (2004).
[2] F. J. Ruess, L. Oberbeck, K. E. J. Goh, M. J. Butcher, E. Gauja, A. R. Hamilton, and M. Y. Simmons, Nanotechnology **16**, 2446 (2005).
[3] M. A. Zudov, C. L. Yang, R. R. Du, T.-C. Shen, J.-Y. Ji, J. S. Kline, and J. R. Tucker, cond-mat/0305482 (unpublished).
[4] K. E. J. Goh, L. Oberbeck, M. Y. Simmons, A. R. Hamilton, and R. G. Clark, Appl. Phys. Lett. **85**, 4953 (2004).
[5] H.-J. Gossmann and F. C. Unterwald, Phys. Rev. B **47**, 12618 (1993).
[6] G. G. Jernigan and P. E. Thompson, J. Vac. Sci. Technol. A **19**, 2307 (2001).
[7] L. Oberbeck, N. J. Curson, M. Y. Simmons, R. Brenner, A. R. Hamilton, S. R. Schofield, and R. G. Clark, Appl. Phys. Lett. **81**, 3197 (2002).
[8] R. J. Hamers and U. K. Köhler, J. Vac. Sci. Technol. A **7**, 2854 (1989).
[9] M. L. Jacobson, M. C. Chiu, and J. E. Crowell, Langmuir **14**, 1428 (1998).
[10] H. F. Wilson, O. Warschkow, N. A. Marks, S. R. Schofield, N. J. Curson, P. V. Smith, M. W. Radny, D. R. McKenzie, and M. Y. Simmons, Phys. Rev. Lett. **93**, 226102 (2004).
[11] Note that 1 ML$=6.8\times 10^{14}$ cm^{-2}.
[12] S. R. Schofield, N. J. Curson, M. Y. Simmons, F. J. Ruess, T. Hallam, L. Oberbeck, and R. G. Clark, Phys. Rev. Lett. **91**, 136104 (2003).
[13] F. J. Ruess, L. Oberbeck, M. Y. Simmons, K. E. J. Goh, A. R. Hamilton, T. Hallam, S. R. Schofield, N. J. Curson, and R. G. Clark, Nano Lett. **4**, 1969 (2004).
[14] Y. Wang, X. Chen, and R. J. Hamers, Phys. Rev. B **50**, 4534 (1994).
[15] K. E. J. Goh, L. Oberbeck, and M. Y. Simmons, Phys. Status Solidi A **202**, 1002 (2005).
[16] M. L. Colaianni, P. J. Chen, and J. J. T. Yates, J. Vac. Sci. Technol. A **12**, 2995 (1994).
[17] D.-S. Lin, T.-S. Ku, and T.-J. Sheu, Surf. Sci. **424**, 7 (1999).
[18] S. Agan, O. A. Mironov, E. H. C. Parker, T. E. Whall, C. P. Parry, V. Y. Kashirin, Y. F. Komnik, V. B. Krasovitsky, and C. J. Emeleus, Phys. Rev. B **63**, 075402 (2001).
[19] P. M. Fahey, P. B. Griffin, and J. D. Plummer, Rev. Mod. Phys. **61**, 289 (1989).
[20] G. Qian, Y.-C. Chang, and J. R. Tucker, Phys. Rev. B **71**, 045309 (2005).
[21] N. L. Mattey, T. E. Whall, R. A. Kubiak, and M. J. Kearney, Semicond. Sci. Technol. **7**, 604 (1992).
[22] We expect strong intersubband scattering in our samples as τ is $\sim 10^{-14}$ s (see Table I) corresponding to an energy uncertainty ($\sim \hbar/\tau$) of ~ 100 meV which is comparable to the energy difference between the occupied subbands for the Si:P δ-doped system (Ref. 20).
[23] We have also performed the same analysis with a valley degeneracy of 2 which is more common for 2D systems in Si and

found no qualitative difference in the transport trends. Quantitatively, the transport parameters are altered by a factor no more than 2.

[24] S. Iwabuchi and Y. Nagaoka, J. Phys. Soc. Jpn. **58**, 1325 (1989).

[25] T. Ando, Rev. Mod. Phys. **54**, 437 (1982).

[26] C. W. J. Beenakker and H. V. Houten, Solid State Phys. **44**, 1 (1991).

[27] S. Hikami, A. I. Larkin, and Y. Nagaoka, Prog. Theor. Phys. **63**, 707 (1980).

[28] A. Kawabata, J. Phys. Soc. Jpn. **53**, 3540 (1984).

[29] We found that fixing or floating the value of α during fitting did not change the trends for τ, τ_φ, and l_φ. In addition, we have also fitted our data with Kawabata's (Ref. 28) formula for $\delta\sigma_{\mathrm{WL}}$ which is also valid beyond the diffusive regime and found excellent agreement with the results from fitting with Hikami's formula.

[30] I. L. Aleiner, B. L. Altshuler, and M. E. Gershenson, Waves Random Media **9**, 201 (1999).

[31] V. Senz, T. Heinzel, T. Ihn, K. Ensslin, G. Dehlinger, D. Grützmacher, and U. Gennser, Phys. Rev. B **61**, R5082 (2000).